Ultrasonics 101 (2020) 106000

Contents lists available at ScienceDirect

Ultrasonics

journal homepage: www.elsevier.com/locate/ultras

Defect reconstruction by non-destructive testing with laser induced ultrasonic detection

Hossam Selim[a,*], Miguel Delgado-Prieto[b], Jose Trull[a], Rubén Picó[c], Luis Romeral[b], Crina Cojocaru[a]

[a] Physics Department, Universitat Politècnica de Catalunya, Rambla Sant Nebridi 22, 08222 Terrassa, Barcelona, Spain
[b] Electronic Engineering Department, Universitat Politècnica de Catalunya, Rambla Sant Nebridi 22, 08222 Terrassa, Barcelona, Spain
[c] Instituto de Investigación para la Gestión Integrada de Zonas Costeras, Universitat Politècnica de València, Paranimf 1, Grao de Gandia, 46730 València, Spain

ARTICLE INFO

Keywords:
Laser ultrasonics
Defect reconstruction
Non-destructive testing
Synthetic aperture focusing technique
2D Apodization
NDT
SAFT
B-scan

ABSTRACT

This work envisages a detailed study of two-dimensional defect localization and reconstruction, using laser generated ultrasound and its application as a remotely controlled non-destructive testing method. As an alternative to full ultrasonic or full optical approaches, we propose a hybrid configuration where ultrasound is generated by impact of laser pulses, while the detection is done with conventional transducers. We implement this approach for defect reconstruction in metallic elements and show that it combines advantages of both photonic and ultrasonic devices, reducing the drawbacks of both methods. We combine our experimental results with a high-resolution signal processing procedure based on the synthetic aperture focusing technique for the benefit of the final two-dimensional visualization of the defects.

1. Introduction

Non-Destructive Testing (NDT) methods are nowadays implemented in industrial applications for the detection of fractures and defects in different materials [1]. The most extended NDT techniques involve transducers generating ultrasound waves and detecting them after the propagation through the material [2]. Typically, they excite ultrasound using conventional transducers placed in contact with the sample and they analyze the ultrasonic pulse's Time Of Flight (TOF) through the material under test from the transducer to the receiver in order to identify discontinuities in the wave propagation. This approach was extensively discussed in many research papers where defects were localized in space, e.g. the measurement of the crack location, height and width [3–5], or of the crack penetration, using ultrasonic guided waves [6]. The detection commonly relies on pulse-echo or pitch-catch modes. Pulse-echo mode uses the same ultrasonic transducer to generate and detect the signals and for a good detection, the defect should be vertically aligned with the sensor. The pitch-catch mode uses an emitter and a receiver and has more flexibility to work both in transmission and reflection modes. This technique can take measurements at different angles, but it is more expensive as it requires many sensors and more complex data processing [7,8]. Ultrasonic signal frequency, ranging from fractions of MHz up to 20 MHz, affects the sensitivity and resolution of the measurement. At higher frequencies, smaller defects can be detected more accurately, but also surface scattering reduces the penetration depth. These methods have the advantages of low cost, easy implementation and provide satisfactory results in many applications. Among the drawbacks we mention low output power preventing such systems to be used remotely, low frequency bandwidth range that makes necessary the use of transducer arrays, small excitation areas that prevent covering large object areas at once and require ultrasonic scanners, and quite low spatial resolution in the excited volume and in the detection.

As an alternative, all-optical methods known as laser-ultrasonics, based on laser generated ultrasound waves and optical detection of the propagated waves, showed up in the NDT field, offering the possibility of remote excitation and detection at a much higher resolution [9,10]. The laser pulse is rapidly absorbed into a shallow volume of the material inducing a stress wave that generates an acoustic pulse [10]. The detection of the transmitted and/or reflected signals can be done as well using optical systems detecting the vibration created by the acoustic wave at the surface, as for example optical interference [11] or techniques of holographic interferometry [9]. All-optical methods have important advantages such as the remote non-contact application and

* Corresponding author.
E-mail addresses: hossam.eldin.mohamed.selim@upc.edu (H. Selim), miguel.delgado@upc.edu (M. Delgado-Prieto), jose.francisco.trull@upc.edu (J. Trull), rpico@fis.upv.es (R. Picó), luis.romeral@upc.edu (L. Romeral), crina.maria.cojocaru@upc.edu (C. Cojocaru).

https://doi.org/10.1016/j.ultras.2019.106000
Received 11 January 2019; Received in revised form 19 June 2019; Accepted 28 August 2019
Available online 31 August 2019
0041-624X/

control, the generation of broadband frequency wave spectrum (from kHz to GHz), high output power and the possibility to easily scan a larger object area at once. As a drawback we mention the critical mechanical stability and the need for an anti-vibration setup in order to obtain reliable results, which make them difficult to apply in certain fields.

In this work, we propose a hybrid system that combines the advantages of the optical systems for remotely laser-generated ultrasonic with conventional transducers for detection. The ultrasound is induced by laser pulses, as in the all-optical methods, allowing inspection from a far distance from the object and enabling a scan of the test specimen remotely, without the need of a direct contact. Laser generated ultrasound also provides a broad frequency bandwidth excitation compared with the limited bandwidth of ultrasonic transducers, covering the whole ultrasonic bandwidth needed for different applications. On the other side, the use of traditional transducers (contact or contact-less) for the ultrasound detection removes the interferometric stability problems in the all-optical techniques. The hybrid system allows an improved measurement of the defects location and size by implementing scan measurements over a specific surface area. We combine our experimental results with a signal processing technique based on synthetic aperture focusing technique (SAFT). SAFT technique is based on the principle of superposition of multiple signals captured at different positions on the surface of the object under test and shifted numerically in time by a delay corresponding to the spatial displacement of the exciters/receivers. This generates a focused image of the defect out of multiple unfocused images. This focused image would have a much higher amplitude at the defect position due to the diffraction of the waves at the defect boundaries compared to healthy positions inside the object of interest. SAFT has the advantage of being able to visualize the whole volume providing two-dimensional (2D) or three-dimensional (3D) information about the object depending on the resolution and the number of scans performed on the object [12–15]. The article is handling the use of laser generated ultrasound (LGU) for NDT applications, achieved through a hybrid system that combines a laser as an ultrasound exciter and contact transducers as receivers. We analyze a metallic cuboid containing an artificially drilled hole representing the defect imbedded inside the material. The recorded data are analyzed by three different algorithms: 1) B-scan analysis that is well known in the literature to scan and detect the position of the defect in one-dimensional (1D) approach [16,17]; 2) 2D SAFT algorithm that is able to generate a 3D reconstructed image of the defect inside the material; 3) an improved 2D SAFT algorithm by using a 2D apodization window, developed by the authors as an expansion to the 1D apodization windows commonly used with 1D SAFT scanning [18–20]. The 2D apodization window allowed to remove redundant shadows and to improve the signal quality in comparison with the first two algorithms. Our main contribution is the reconstruction of the defect by the application of the SAFT algorithm in volumetric regime, with depth information instead of the 2D regimes (only depth plane) we found in the literature. To our knowledge, the articles discussing SAFT algorithm are mainly interested in scanning the receivers across the scan line/area or scanning both exciters and receivers. In this work we perform a remote scan of the exciter (the laser impact pulse) over a 2D area, with a high number of scan points and high step resolution. We could also scan the receiver, using transducers arrays. Instead, we demonstrate that with only two fixed detectors we obtain reasonably good results. Our main goal is to show the proof of concept of our hybrid device along with the B-scan and SAFT algorithms. the 2D apodization applied to the SAFT algorithm improve the data processing and eliminates ultrasound reflections generated by the nature of LGU, the boundary reflections and wide angle between scanning exciter/receiver set.

2. Experimental set-up

The set-up designed for our experiments is shown schematically in Fig. 1. We use an Nd:YAG laser doubled in frequency, emitting pulses of 8 ns at a wavelength of 532 nm, with an energy per pulse of 10 mJ. The focused laser beam impacts onto the surface of the object under study where the pulse is rapidly absorbed into a shallow volume of the material and creates a localized thermo-elastic expansion. This expansion induces a stress wave and an acoustic pulse generating broadband ultrasound waves that propagate inside the material. The laser beam can scan a selected area of the object surface by means of a programmable XY galvanometer. For each excitation point, the ultrasonic waves propagate through the object, they are reflected or scattered by different material particles in the volume, and then is detected by the ultrasonic transducer.

For the detection we use two conventional ultrasonic sensors (Olympus V133-RM) at 2.2 MHz central frequency, coupled to the surface of the object. The sensors can be placed on the incident surface (measuring reflection/scattering) as well as on the opposite side (measuring transmission). The signal collected by the sensors is sent to a preamplifier (Olympus 5662), connected to a high-performance Gage A/D card (50 MHz sampling frequency, 16 bit of resolution), linked to a computer for further data processing. For each excitation point the transducer records a voltage/time (A-scan) data set.

We analyze two aluminum cuboid samples with identical dimensions of 300 mm × 200 mm × 20 mm. One sample is homogeneous, without any holes or defects, referred in the following discussion as “healthy”. The second one, shown in Fig. 2, has a cylindrical hole with a diameter of 8 mm and hole depth of 85 mm and is referred to from now on as the “unhealthy” sample. Two different experiments were performed on this sample: (i) the laser performs a 1D scan (B-scan) and the detection is made with only one transducer; (ii) the laser perform a 2D scan, we use two transducers for detection and we apply SAFT algorithm for the signal processing. The laser scan is performed on the 300 mm × 200 mm face of the cuboid and the receiving transducers are located at the same face of the cuboid where laser excitation is performed, i.e; working in reflection mode. Fig. 2 shows the laser scanning line/area and the sensors' positions in each experiment.

3. B-scan and signal processing

In the first experiment the galvanometer was programmed to execute a 1D scan (B-scan) along one line of the object surface in the horizontal X direction, crossing on top of the defect, Fig. 2a. We selected 120 scan points covering a distance of 80 mm. For each excitation point the ultrasound waves detected by the sensor were recorded using our data acquisition system. For the signal processing we applied a bandpass filter of 3 MHz bandwidth around the 2.25 MHz central frequency and an interpolation algorithm to reduce the excessive oscillation noise and unnecessary perturbations.

The B-scan results for all processed signals are shown in Fig. 3. For the healthy sample in Fig. 3a and for the unhealthy one in Fig. 3b. We plot the position of the scan points as a function of the time of flight (TOF) frames, while the color bar represents the intensity of the signal. A higher intensity is a sign of a high reflection towards the sensor coming from a reflecting source that can be a boundary or a defect embedded in the object under test.

The TOF of the waves depends on the distance between the laser incidence point and the acoustic sensor’s position. The first wavefront arriving from the laser to the sensor starts to appear at $t = 11\mu s$ for both samples, since the relative position of the laser scan line and the sensor was the same. For the healthy sample there is no visible perturbation in the B-scan map, due to the homogeneity of the sample. All reflections come from the borders. For the unhealthy sample we see the same boundary reflections, overlapped with the reflections coming from the defect. The latter ones alter the B-scan map, showing major discontinuities and perturbations that correspond to the effect of the hole. As highlighted in Fig. 3b, the discontinuities clearly appear in the range between $X_1 = 25$ mm and $X_2 = 36$ mm, respectively ($\Delta X = 11$ mm), on

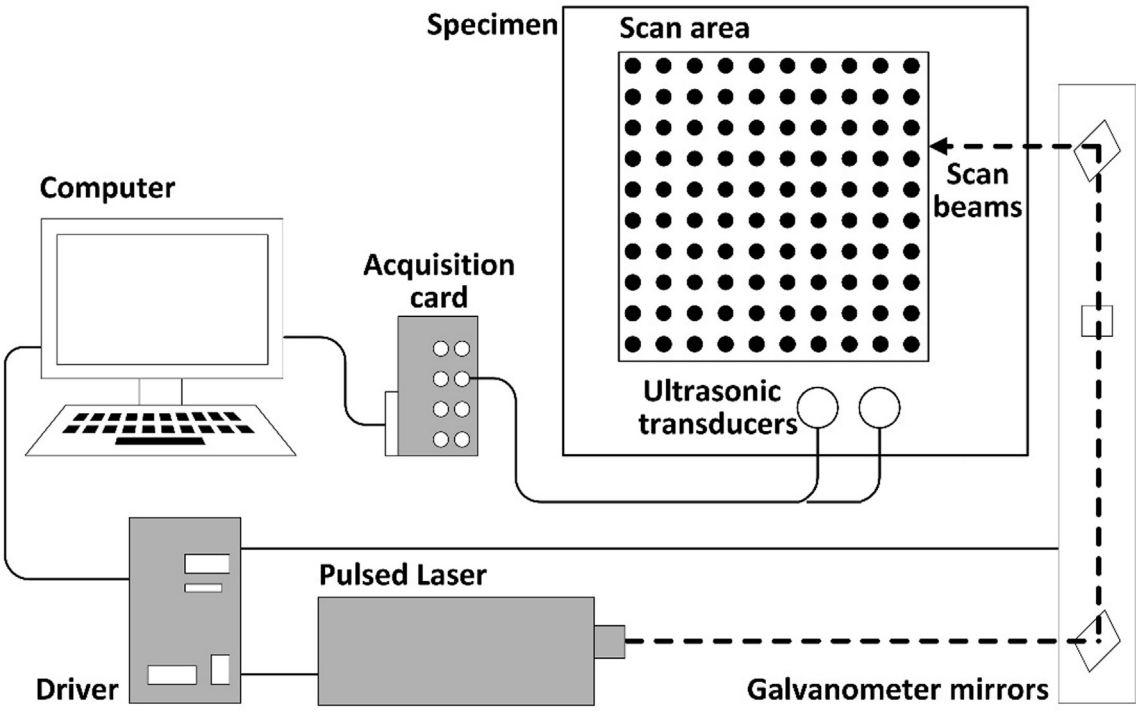

Fig. 1. Schematic representation of the experimental set-up.

the vertical axis and it is centered at scan position X = 30.5 mm.

In order to improve visualization of discontinuities, we added to Fig. 3b an inset for the reader to find out the discontinuities clearly. The color map in the inset of Fig. 3b is reduced to lower bounds to emphasize and exaggerate the color contrast and make it more distinguishable. We need to emphasize that the echoes from the hole are reflected from both the front and rear surfaces of the cylinder. Front surface is providing higher intensity due to this reflection, while the signal passing to the rear surface is already moving in the air in the hole until it reaches the rear surface and then reflected back to the transducer (passing again by the air in the hole). This attenuates the signal and causing lower amplitude for this reflection. Other echoes appearing later in time axis are multiple reflections from defect and boundaries and include a lot of interference, so they are not essential in this analysis. These main reflections are highlighted by the arrows in the larger Fig. 3b with the full color map range.

These values are very close to the actual hole diameter of 8 mm and its position on the sample, with a sizing error of 37% (the defect appears to be bigger than it really is), and a positioning error of 0%.

This first experiment shows that B-scan technique, using a remote

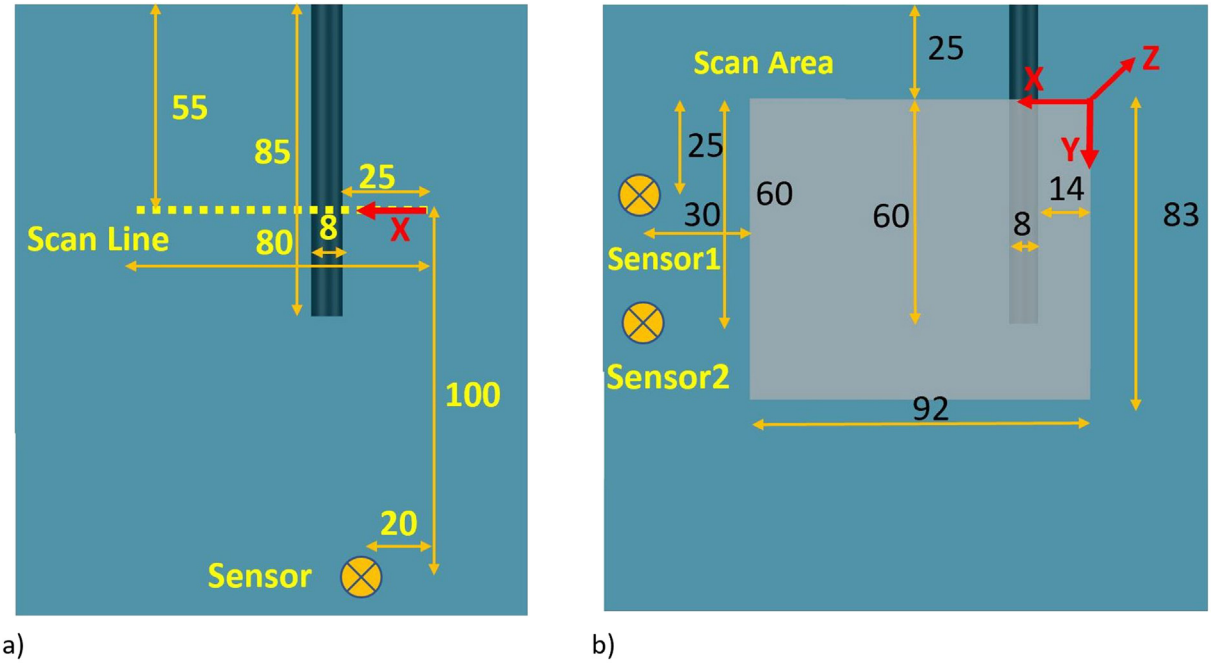

Fig. 2. Experimental schematic diagram with a) scan line and ultrasonic sensor positions for B-scan experiment and b) scan plane in grey for SAFT experiment and ultrasonic sensors for second experiment.

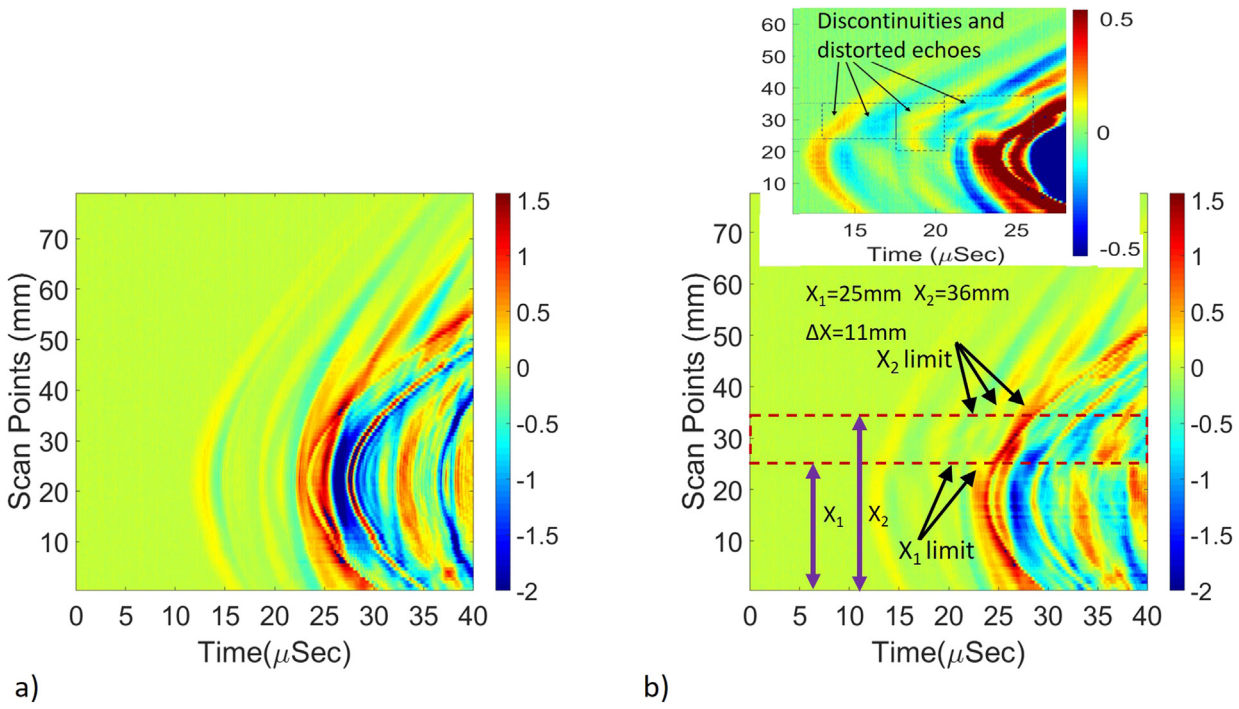

Fig. 3. a) B-scan results of the healthy sample b) B-scan results of the unhealthy sample with an inset zooming the discontinuities.

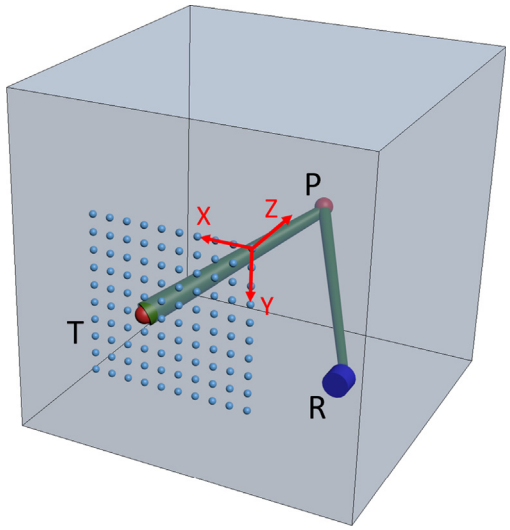

Fig. 4. Scheme of the SAFT technique processing used for the object detection. A wave is sent from a point of interest (P) by a transmitter (T). It is reflected/scattered by the defect and measured at the receiver (R). The procedure is repeated with the transmitter in every point of interest.

1D laser scan and only one sensor, is a very simple and robust technique that provides reliable information about general position of defect location in a fast process. The resolution of the results is comparable with the commercial NDT full ultrasonic devices but have the advantages of noncontact excitation and remote control of the scan. However, this method does not allow a 2D reconstruction of the defect.

4. Two-dimensional scan and SAFT analysis

When a 2D or 3D reconstruction of the defect is envisaged, a 2D scan configuration, easily achievable with our laser induced excitation system, is required. We programmed our experimental setup, shown in Fig. 1, to perform a 2D scan over a MxN matrix points by remotely controlling the position of laser incident point onto the object surface. The scanning area (in grey) as well as the position of the receivers (in yellow) in this second experiment are shown in Fig. 2b. For each excitation point, each receiver records a corresponding A-scan signal. The experimental results combined with the SAFT technique are expected to give accurate information about the area of the defect for getting a precise 2D visualization of its location and dimensions.

SAFT is commonly used for the signal processing in the characterization of embedded defects in the volumetric regime. The technique is based on the delay and sum (DAS) principle, that superimposes the relatively low-resolution A-scan data at every excitation point of the scanned area, creating a higher resolution focused image, with a higher signal to noise ratio (SNR), referred to as the synthetic aperture (SA). Depending on the implemented setup, the analysis can be performed in the time or frequency domain [12–14]. SAFT can generate a 2D image of a particular plane of the object, or can be generalized to the 3D mode to cover all planes in a volume. The reconstructed 3D image can project maps of the defect in any image plane, regardless of the plane used for the scanning of the ultrasonic signals. In the time domain analysis, the TOF is calculated across all SA points, starting from the excitation signal source position at a particular scan index to all geometrical target points in the object's volume and back to the signal receiver, for each particular scan point. For each geometrical point, an integration of all received signals at a particular value of TOF is calculated, to produce the final pixel value of this particular scan point in the final image. This integration results in a higher contrast, resolution and better SNR value [14,15]. Fig. 4 shows a schematic representation of the SAFT technique, assuming a 3D object under investigation with an arbitrary scatter point P and an exciter–receiver set in a pitch-catch mode, similar to our experimental set-up. We consider an arbitrary excitation point T generating spherical waves and a receiver R, both placed on the XY plane. The SA top view is assumed to be on the XY plane.

The $TOF_{(i,j,k)P}$ of the ultrasonic signal generated by T and detected by R after it has been propagated to and reflected by the arbitrary point P, can be calculated as:

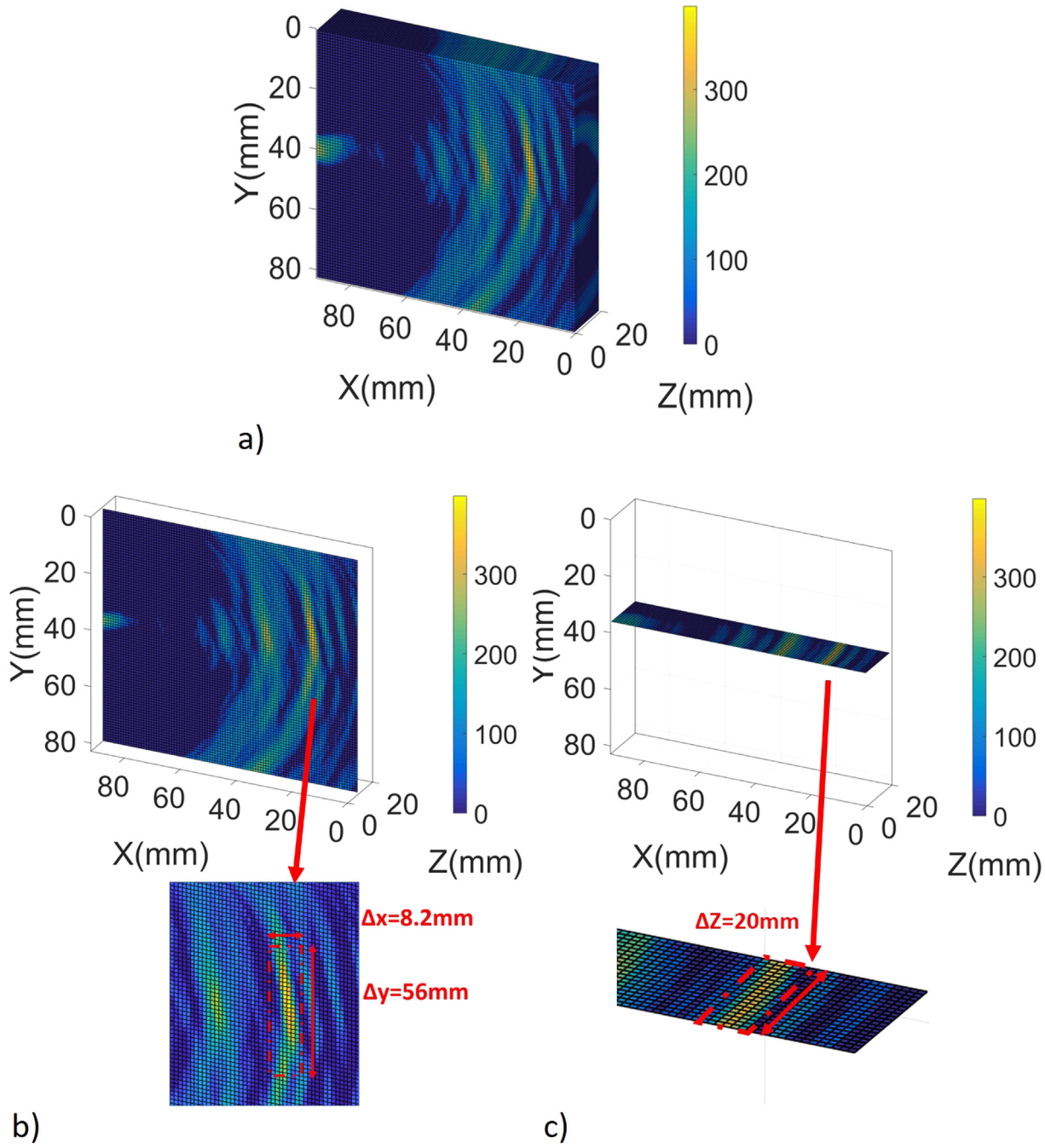

Fig. 5. Reconstruction results of SAFT technique for the thin cuboid with insets to show reconstructed defect dimensions a) 3D volume representation b) 3D slice for XY plane c) 3D slice for XZ plane.

$$TOF_{(i,j,k)_P} = \frac{|\vec{d}_{(i,j,k)_P} - \vec{d}_{(i,j,0)_T}| + |\vec{d}_{(i,j,k)_P} - \vec{d}_{(i,j,0)_R}|}{c} \quad (1)$$

where d is the displacement vector at T, R and P positions, i, j, k are the indexes of the volume image points in the X, Y, Z planes respectively, and c denotes the speed of the longitudinal waves in the material [12,21–23]. This calculation is done for every point in the A-scan measurements to produce a preliminary unfocused image y_R of this particular point P. The combination of all individual images results into a high resolution focused image y_f. We assume that the scan is done for MxN points denoting the number of the 2D excitation steps over the SA, and that only one receiver collects all the transmitted A-scan data from all scan points at an arbitrary point in the SA. The final signal is given by:

$$y_f\left(\vec{R_P}\right) = \sum_{j=1}^{N} \sum_{i=1}^{M} y_R\left(TOF_{(i,j,k)_P}, i, j\right) \quad (2)$$

where y_R is the measured A-scan signal amplitude at the corresponding $TOF_{(i,j,k)P}$ at scan point i and $j$and y_f is the focused signal received from all the scan points at this particular receiver R. This can be regarded as an integration of all received signals from MxN excitation points at the SA.

In Eq. (2) we need to add a coefficient that represents the effect of the attenuation and decay in the acquired signal when it passes from the exciter to the scattered point and back to the receiver. This coefficient is called weighting function or apodization function: a(TOF$_{(i,j,k)P}$,i,j) [21].

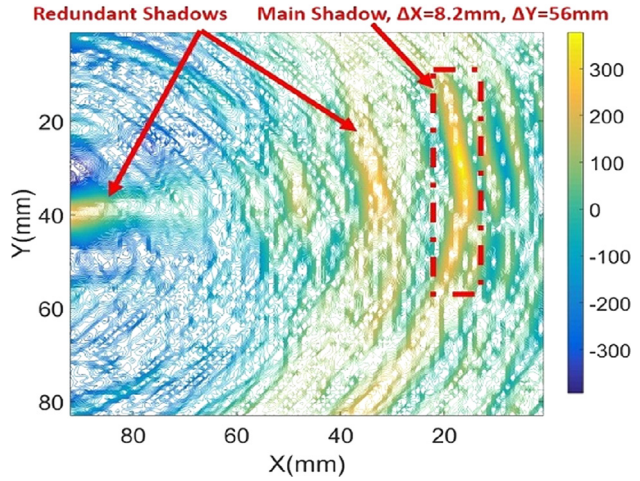

Fig. 6. Contour map of the defect at XY plane at Z = 10 mm using SAFT technique.

$$y_f\left(\vec{R_P}\right) = \sum_{j=1}^{N}\sum_{i=1}^{M} a\left(TOF_{(i,j,k)P},\, i,\, j\right) * y_R\left(TOF_{(i,j,k)P},\, i,\, j\right) \tag{3}$$

In order to account for the diffraction in propagation, the apodization function applies lower weights to the captured signals at the far ends of SA and filters the unfocused signals in the SAFT analysis. Eq. (3) represents the DAS where summation is applied to the delayed versions of the signals at the corresponding scan points.

The focused signal results from the superposition of the A-scan data from MxN excitation points captured by one receiver, where each A-scan itself is a superposition of signals coming from point scatters in the whole volume. If we go further and we assume that we could implement also a MxN scanning matrix for the receiver position, Eq. (3) can be modified to consider the integration of all receivers as well. In this case each image point will be constructed from $(MxN)^2$ points of integration instead of MxN scan points as for the case when we use only one receiver. SAFT can, thus, be applied to any image of all planes to produce an image for the defect from any projection direction.

There are several assumptions that we have to make when we apply SAFT to the final image reconstruction. The exciter is considered to be a point source, which perfectly applies for the laser generated ultrasound. Receivers are assumed to be point-like transducer: the smaller the size, the less numerical errors in the algorithm. The laser scanning area and the receiver locations are assumed to be far enough from the object's boundaries to avoid reflections that could cause misleading data. The medium is assumed to be homogeneous, with non-spatial dependent physical parameters. In other scenarios where the wave dispersion could be significant due to the presence of composite or inhomogeneous materials, the SAFT algorithm should be modified to account for different wave velocities and wave diffraction.

Experimental measurements have been conducted in a pitch-catch mode for two different objects. the first object is a thin cuboid with small depth and the second object is a larger cube. This was done to compare the results of the reconstructed image of the defect with reference to the object dimensions. The first experiment was conducted on the thin cuboid object using two receivers placed at the fixed positions indicated in Fig. 2b. The laser has been programmed to scan an area of 92 mm × 83 mm, with 101 × 91 scan points. The signals captured by the two sensors have been recorded using the amplifier and data acquisition system described in Section 3, and were pre-processed using a band pass filter and an interpolation algorithm to remove the background noise and low/high frequency components. Then, an averaging algorithm was applied to remove the DC components from the signal. The SAFT algorithm was finally applied. A Gaussian filter was used to enhance the reconstructed image.

The reason we did not add more receivers (e.g: microphone array) is that our main goal is to use the transmitter, not the receiver, as the scanning mechanism with a lot of points with high step resolution. With laser excitation, we can do the scanning of the transmitter with a step size of 0.9 mm for more than 9000 scan points. This is very difficult to achieve with conventional arrays. In addition, the scanning with the laser makes the incident pulse on the object surface equivalent to a point source, which is better for the SAFT efficiency.

As a result, we obtain the volume reconstruction of the selected scanned area shown in Fig. 5a, where the defect corresponds to the yellow shadows. The position and dimensions of the defect can be better visualized and measured if we select projections of different cross-sections in the volume of interest, that can be extracted from Fig. 5 for any required coordinates. Fig. 5b and c show two cross-section slices in the XY and XZ planes respectively. From these projections we measure a defect with horizontal (ΔX) size of 8.2 mm and vertical (ΔY) size of 56 mm. The apodization function $a(TOF_{(i,j,k)_P}, i, j)$ in Eq. (3) was not used in this analysis. It is going to be used later in the next section in the improved algorithm.

The contour map of one of the cross-sections is another representation of the results that can even better visualize the defect. Fig. 6 shows the contour map of the XY cross-section, enabling the reconstruction of the X and Y dimensions: the defect is centered at X = 17.5 mm and Y = 40 mm with the corresponding size ΔX = 8.2 mm and ΔY = 56 mm. Compared with the real size and position of the defect in our sample, the resulting reconstruction has the following errors: a sizing error of 4.6%, concretely, ΔX_{error} = 2.5% and ΔY_{error} = 6.7% and a positioning error of 12.25%, concretely, X_{error} = 2.5% and Y_{error} = 22%. There are other reflections in the resulting images with lower amplitude that do not come from the defect, that could be misleading eve though they are at low intensity in comparison to the main shadow that can be significantly distinguished as the main defect. The contour map helped to identify and ignore these redundant shadows. These reflections and redundant shadows are overcome in the next section by considering a modified SAFT algorithm.

The redundant reflections shown in Figs. 5 and 6 appear due to two constraints of our experimental configuration. On one hand, our object has one small dimension Z compared with the X and Y ones making the distance between the laser/sensor and the defect larger than the distance to the Z boundaries of the object. This results in multiple reflections which arrive to the receiver faster than those coming from the defect. leading to misleading wavefronts that produce shadows in the reconstructed image. This constraint, that applies to all object boundaries in all directions, can be eliminated if we are able to avoid internal reflections from the boundaries. On the other hand, the fact that the position of the sensors is fixed while we scan the laser pulses results in an angular change between the excitation and detection. At large angles, the performance of the SAFT technique is reduced and can significantly decrease the signal-to-noise ratio. In addition, side lobes of the LGU could add other shadows to the reconstructed images. These constraints can be resolved by increasing the object's depth and reducing the angle by scanning the receivers along with the laser beam [24–27].

We can improve SAFT algorithm results by applying a 2D apodization technique that can reduce the redundant shadows as described in the next section.

5. Two-dimensional apodization for improved SAFT analysis

The apodization function $a(TOF_{(i,j,k)_P}, i, j)$ in Eq. (3) was not yet used in the previous SAFT analysis. Its implementation in the algorithm removes the redundant shadows appearing in the reconstructed images shown in Figs. 5 and 6. First of all, we applied a narrow bandpass filter with cut off frequencies (1 MHz to 2.5 MHz) to the directly captured A-scan raw data as a pre-processing filter before applying the SAFT

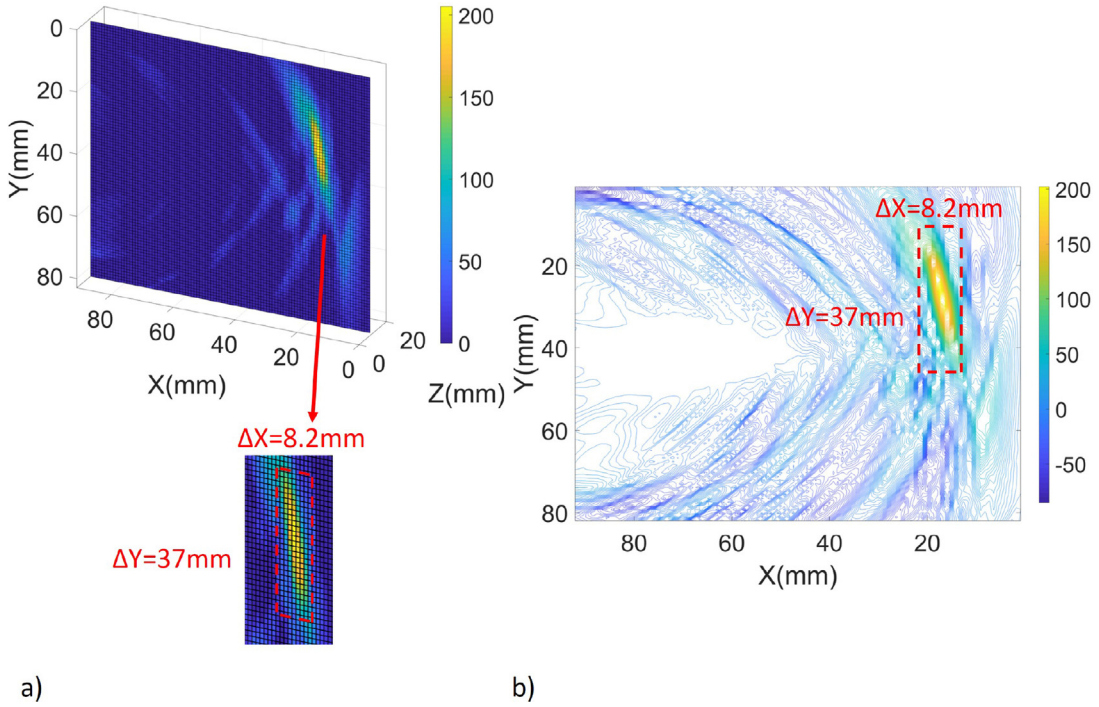

Fig. 7. Reconstruction of the defect using improved SAFT technique after applying narrow band-pass frequency filter and 2D apodization function a)3D slice for XY plane b) slice Contour map of the defect at XY plane at Z = 10 mm.

algorithm. We then included the apodization function at Eq. (3) which adds weights to the summation of the recorded signals at specific times of light in order to magnify the effect of the signals within the apodization window and eliminate those falling outside the window limits [18–20,28,29]. 1D apodization function is used when a line scan is executed, as described in the literature. Here in our case where an area scan is used of a line scan, the apodization window needs to get expanded as well from a line to an area. The 2D expansion has been applied to improve the apodization algorithm from the traditional 1D approach known in the literature to the general 2D approach [18]. The size of the apodization function needs to change with respect to the depth of the scatterer points in the scan volume to cover the synthetic aperture area. Rectangular and Hanning apodization functions are commonly used in the SAFT analysis [19,20]. Full details about the theoretical background and derivation of the apodization function for 1D and 2D windows can be found in [18]. In this article, we focus on the final derived equations that are going to be used for our SAFT analysis [18]. considering a scanner/receiver at position (X′,Y′) with respect to a point scatterer at the volume of the object at position (X, Y,Z) where Z represents the depth of the point scatterer, and $\Delta X(Z)$ and $\Delta Y(Z)$ are the widths of the apodization windows in the X and Y axes directions respectively, we can represent the normalized coordinates of the scatterers as:

$$\hat{X} = \frac{X - X'}{\Delta X(Z)} \tag{4}$$

$$\hat{Y} = \frac{Y - Y'}{\Delta Y(Z)} \tag{5}$$

Thus, the final apodization function can be represented by:

$$a(\hat{r})_{Hann} = \begin{cases} 0.5[1 + \cos(\frac{\pi}{\alpha}\hat{r})], & |\hat{r}| < \alpha \\ 0, & otherwise \end{cases} \tag{6}$$

where $\hat{r} = \sqrt{\hat{X}^2 + \hat{Y}^2}$ can represent the 2D expansion of the apodization window. substituting the values of X′, Y′, X, Y and Z from Eq. (6) by the indexes i,j,k in the factor $a(TOF_{(i,j,k)_p}, i, j)$ in Eq. (3), would solve the main SAFT equations with the weighting and apodization windows applied to all point scatterers in the volume of interest. we use the Hann window with a threshold criterion $\alpha = 0.8$ after proper fine tuning that provided the optimum signal to noise ratio and enhanced the resulting reconstructed image with no redundant shadows.

Applying this apodization function at all point scatterers, we can find the resulting reconstructed image as in Fig. 7a, where one can note that all the redundant shadows have been eliminated and only the main shadow appears, with a high signal quality. The contour map in Fig. 7b emphasizes this effect showing only the contour lines of the main shadow. The apodization function clearly improves the reconstructed defect image in comparison with the results shown in Figs. 5 and 6.

The defect is centered at X = 17.5 mm, Y = 30 mm and Z = 10 mm with the corresponding size ΔX = 8.2 mm and ΔY = 37 mm. Compared with the real size and position of the defect in our sample, the resulting reconstruction has the following size errors $\Delta X_{error} = 2.5\%$ and $\Delta Y_{error} = 38\%$ and position errors $X_{error} = 2.5\%$ and $Y_{error} = 0\%$.

We obtain an improvement in the position error, while the size error increased slightly but still remains within satisfactory limits. The results we obtained with the 2D apodization function added a power to the SAFT algorithm with enhanced results overcoming the challenging constraints of the experimental configuration.

6. Conclusion

We applied and compared three different techniques for defect localization and reconstruction, using a hybrid system composed by laser generated ultrasound and conventional transducer receivers. The results obtained with the three methods, the B-scan, the SAFT technique and the improved SAFT technique with 2D apodization function, indicate similar position of the defect, confirming the reliability of the algorithms. B-scan measurements allow the defect reconstruction only from one perspective, and with a limited resolution. The implementation of the 2D scanning area and the signal processing using the SAFT technique over the object's volume allows the defect visualization from different angles and at different depths, making possible a 3D image reconstruction. We used the discussed algorithms to localize the defect

position with a good signal-to-noise ratio, taking into consideration the limitations of structural dimensions. The resolution of the reconstruction is in a range between those of the classical ultrasonic and the full optical methods. Boundary reflections, side lobes of the laser generated ultrasound and angle between exciters and receivers influence the quality of the resulting reconstructed image of the defect. when considered carefully, using 2D apodization function, the redundant shadows are removed and only the main shadow corresponding to the defect is generated. We believe that this hybrid approach combines different advantages of both photonic and ultrasonic devices, reducing the drawbacks of both methods. The remote control of the broad band excitation, possibility of scanning large areas and reduced number of receivers make it easy to implement for different materials and applications.

Acknowledgements

The work was supported by Spanish Ministry of Economy and Innovation (MINECO) and European Union FEDER through project FIS2015-65998-C2-1 and FIS2015-65998-C2-2 and by project AICO/2016/060 by Consellería de Educación, Investigación, Cultura y Deporte de la Generalitat Valenciana.

References

[1] S.C. Her, S.T. Lin, Non-destructive evaluation of depth of surface cracks using ultrasonic frequency analysis, Sensors (Switzerland) 14 (9) (2014) 17146–17158, https://doi.org/10.3390/s140917146.

[2] B. Mi, J.E. Michaels, T.E. Michaels, An ultrasonic method for dynamic monitoring of fatigue crack initiation and growth, J. Acoust. Soc. Am. 119 (1) (2006) 74–85, https://doi.org/10.1121/1.2139647 <http://asa.scitation.org/doi/10.1121/1.2139647>.

[3] S. Ham, H. Song, M.L. Oelze, J.S. Popovics, A contactless ultrasonic surface wave approach to characterize distributed cracking damage in concrete, Ultrasonics 75 (2017) 46–57, https://doi.org/10.1016/j.ultras.2016.11.003.

[4] U. Amjad, S.K. Yadav, T. Kundu, Detection and quantification of pipe damage from change in time of flight and phase, Ultrasonics 62 (2015) 223–236, https://doi.org/10.1016/j.ultras.2015.05.022.

[5] M. Kharrat, L. Gaillet, Non-destructive evaluation of anchorage zones by ultrasonics techniques, Ultrasonics 61 (2015) 52–61, https://doi.org/10.1016/j.ultras.2015.03.007.

[6] B. Masserey, C. Raemy, P. Fromme, High-frequency guided ultrasonic waves for hidden defect detection in multi-layered aircraft structures, Ultrasonics 54 (2014) 1720–1728, https://doi.org/10.1016/j.ultras.2014.04.023.

[7] S. Delrue, K. Van Den Abeele, E. Blomme, J. Deveugele, P. Lust, O.B. Matar, Two-dimensional simulation of the single-sided air-coupled ultrasonic pitch-catch technique for non-destructive testing, Ultrasonics 50 (2) (2010) 188–196, https://doi.org/10.1016/j.ultras.2009.08.005.

[8] S. Delrue, M. Tabatabaeipour, J. Hettler, K. Van Den Abeele, Applying a nonlinear, pitch-catch, ultrasonic technique for the detection of kissing bonds in friction stir welds, Ultrasonics 68 (2016) 71–79, https://doi.org/10.1016/j.ultras.2016.02.012.

[9] T. Kreis, Application of digital holography for nondestructive testing and metrology: a review, IEEE Trans. Industr. Inf. 12 (1) (2016) 240–247, https://doi.org/10.1109/TII.2015.2482900.

[10] K. Zhang, Z. Zhou, J. Zhou, Application of laser ultrasonic method for on-line monitoring of friction stir spot welding process, Appl. Opt. 54 (25) (2015) 7483–7489, https://doi.org/10.1364/AO.54.007483 <http://ao.osa.org/abstract.cfm?URI=ao-54-25-7483>.

[11] Y.K. Zhu, G.Y. Tian, R.S. Lu, H. Zhang, A review of optical NDT technologies, Sensors 11 (8) (2011) 7773–7798, https://doi.org/10.3390/s110807773.

[12] S. Boonsang, J. Zainal, R.J. Dewhurst, Synthetic aperture focusing techniques in time and frequency domains for photoacoustic imaging, Insight: Non-Destruct. Test. Condit. Monit. 46 (4) (2004) 196–199, https://doi.org/10.1784/insi.46.4.196.55648.

[13] M. Spies, H. Rieder, Synthetic aperture focusing of ultrasonic inspection data to enhance the probability of detection of defects in strongly attenuating materials, NDT and E Int. 43 (5) (2010) 425–431, https://doi.org/10.1016/j.ndteint.2010.04.002.

[14] A. Ganguli, C.M. Rappaport, D. Abramo, S. Wadia-Fascetti, Synthetic aperture imaging for flaw detection in a concrete medium, NDT and E Int. 45 (1) (2012) 79–90, https://doi.org/10.1016/j.ndteint.2011.09.004.

[15] A.N. Sinclair, J. Fortin, B. Shakibi, F. Honarvar, M. Jastrzebski, M.D.C. Moles, Enhancement of ultrasonic images for sizing of defects by time-of-flight diffraction, NDT and E Int. 43 (3) (2010) 258–264, https://doi.org/10.1016/j.ndteint.2009.12.003.

[16] K.A. Tiwari, R. Raisutis, O. Tumsys, A. Ostreika, K. Jankauskas, J. Jakutavicius, Defect estimation in non-destructive testing of composites by ultrasonic guided waves and image processing, Electronics 8 (3) (2019) 315, https://doi.org/10.3390/electronics8030315.

[17] K.A. Tiwari, R. Raisutis, V. Samaitis, Hybrid signal processing technique to improve the defect estimation in ultrasonic non-destructive testing of composite structures, Sensors (Switzerland) 17 (12) (2017) 2858, https://doi.org/10.3390/s17122858.

[18] H. Selim, J. Trull, M. Delgado Prieto, R. Picó, L. Romeral, C. Cojocaru, Fully non-contact hybrid NDT for 3D defect reconstruction using SAFT algorithm and 2D apodization window, Sensors (Basel, Switzerland) 19 (9) (2019), https://doi.org/10.3390/s19092138.

[19] H.S. Martin, Synthetic Aperture Ultrasound Imaging with Application to Interior Pipe Inspection, University of Tromsø, 2012, pp. 1–135 (September).

[20] Wulang Widada, Two Dimensional Window Functions, Thesis, Naval Postgraduate School, 1979.

[21] J.A. Jensen, S.I. Nikolov, K.L. Gammelmark, M.H. Pedersen, Synthetic aperture ultrasound imaging, Ultrasonics 44 (SUPPL.) (2006), https://doi.org/10.1016/j.ultras.2006.07.017.

[22] M. Spies, H. Rieder, A. Dillhöfer, V. Schmitz, W. Müller, Synthetic aperture focusing and time-of-flight diffraction ultrasonic imaging - Past and present, J. Nondestr. Eval. 31 (2012,) 310–323, https://doi.org/10.1007/s10921-012-0150-z.

[23] T. Stepinski, F. Lingvall, Synthetic aperture focusing techniques for ultrasonic imaging of solid objects, in: 2010 8th European Conference on Synthetic Aperture Radar (EUSAR), 2010, pp. 1–4. doi: papers2://publication/uuid/72BB2E26-227F-4027-9433-3990165E5916. http://ieeexplore.ieee.org/xpls/abs_all.jsp?arnumber=5758760.

[24] I.I. Matsuya S., Matozaki K., Directivity Patterns of Ultrasound Generated by Evanescent light at the Interface between Prism and Aluminum Surface, vol. 34, 2013, pp. 205–206.

[25] P. Zhang, C.F. Ying, J. Shen, Directivity patterns of laser thermoelastically generated ultrasound in metal with consideration of thermal conductivity, Ultrasonics 35 (3) (1997) 233–240, https://doi.org/10.1016/S0041-624X(96)00106-0.

[26] V.V. Krylov, Directivity patterns of laser-generated sound in solids: Effects of optical and thermal parameters, Ultrasonics 69 (2016) 279–284, https://doi.org/10.1016/j.ultras.2016.01.011 arXiv:1402.6024.

[27] J. Li, H. Zhang, C. Ni, Z. Shen, Analysis of laser generated ultrasonic wave frequency characteristics induced by a partially closed surface-breaking crack, Appl. Opt. 52 (18) (2013) 4179–4185, https://doi.org/10.1364/AO.52.004179 <http://ao.osa.org/abstract.cfm?URI=ao-52-18-4179>.

[28] T.L. Szabo, Diagnostic Ultrasound Imaging: Inside Out: Second Edition, 2004. https://doi.org/10.1016/C2011-0-07261-7.

[29] R.S.C. Cobbold, Corrections to Foundations of Biomedical Ultrasound, Oxford University Press, 2013, pp. 1–5.